The role of the $\Lambda(1405)$ in the $pp \to pK^+\Lambda(1405)$ reaction

L. S. Geng* and E. Oset†
Departamento de Física Teórica and IFIC, Centro Mixto,
Institutos de Investigación de Paterna - Universidad de Valencia-CSIC, Valencia, Spain

We report a theoretical study of the $pp \to pK^+\Lambda(1405)$ reaction, which was recently investigated at COSY-Jülich by using a 3.65 GeV/c circulating proton beam incident on an internal hydrogen target. The reaction is driven by single kaon exchange, single pion exchange, and single rho exchange terms which have very different shapes due to the two pole structure of the $\Lambda(1405)$ and the presence of background terms. The shape for the sum of the three contributions, as well as the total cross section, are consistent with present data within experimental and theoretical uncertainties, using reasonable form factors for the meson-baryon vertices.

PACS numbers: 13.75.-n, 13.30.-a, 14.20.Jn

I. INTRODUCTION

The $\Lambda(1405)$ has been a rather controversial resonance for a long time. In most quark-model calculations, it is described as a p-state q^3 baryon with mainly a SU(3) singlet structure [1]. On the other hand, in Refs. [2, 3], the $\Lambda(1405)$ is believed to be a resonance emerging from the interaction of the $\bar{K}N$ and $\pi\Sigma$ systems, and therefore of $q^4\bar{q}$ structure. Recent studies based on unitary chiral theory, UχPT [4, 5, 6, 7, 8, 9, 10, 11], in particular favor this interpretation. Furthermore, the models based on UχPT predict that the nominal $\Lambda(1405)$ is a superposition of two resonances: one around $1390 - i66$ MeV and the other around $1426 - i16$ MeV [7, 8]. More recently, the studies of the $\bar{K}N$ interaction have been extended by including higher order chiral Lagrangians in the kernel of the interaction [12, 13, 14, 15]. The position of the high-energy pole is rather similar in all these works, but there are variations in the position of the low-energy pole. Nevertheless, the theoretical uncertainties have been studied in [15] and the results obtained with the lowest-order chiral Lagrangians [7, 8] are well within the uncertainties of these extended models [12, 13, 14, 15].

As first demonstrated in Ref. [8], due to the fact that the two poles of the $\Lambda(1405)$ couple differently to the $\bar{K}N$ and $\pi\Sigma$ channels (the high-energy pole couples more to the $\bar{K}$N channel whereas the low-energy pole more to the $\pi\Sigma$ channel), different production mechanisms may favor one channel or the other and lead to different invariant mass distributions, thus offering the possibility to experimentally test the two-pole prediction. The reactions $\gamma p \to K^+\Lambda(1405)$ and $K^-p \to \Lambda(1405)\gamma$, (particularly the latter one), are shown to be sensitive to the high-energy pole of the $\Lambda(1405)$ and thus the corresponding invariant mass distributions exhibit a peak at ~ 1420 MeV [16, 17]. On the other hand, the reaction $\pi^-p \to K^0(\Sigma\pi)^0$ seems to give more weight to the low-energy pole and thus exhibits a peak around 1390 MeV in the $\pi\Sigma$ invariant mass distributions [18]. Recently, we have shown that the two-pole structure may also lead to quite different radiative decay widths [19].

The two-pole structure of the $\Lambda(1405)$ has inspired several experimental studies [20]. The Crystal Ball Collaboration has measured the reaction $K^-p \to \pi^0\pi^0\Sigma^0$ [21]. In Ref. [22] it was shown that the measured invariant mass distribution supports the two-pole structure of the $\Lambda(1405)$.

I. Zychor et al. have recently studied the reaction $pp \to pK^+\Lambda(1405)$ at COSY-Jülich by using a 3.65 GeV/c circulating proton beam on an internal hydrogen target [23]. By means of invariant- and missing-mass techniques, they were able to separate the overlapping $\Sigma^0(1385)$ and $\Lambda(1405)$. The shape and position of the $\Lambda(1405)$ constructed from its $\pi^0\Sigma^0$ decay channel are claimed to be consistent with the data from the $\pi^-p \to K^0(\Sigma\pi)^0$ reaction [24] and the $K^-p \to \pi^+\pi^-\Sigma^+\pi^-$ reaction [25].

It is the main purpose of this paper to study theoretically the $pp \to pK^+\Lambda(1405)$ reaction. In sect. II we give a brief description of unitary chiral theory and the two $\Lambda(1405)$'s. In sect. III we investigate possible reaction mechanisms, and build a model based on unitary chiral theory to study the reaction $pp \to pK^+\Lambda(1405)$. In sect. IV, we compare the calculated invariant mass distribution with the data and we show that our model reproduces rather well both the total cross section and the invariant mass distribution within the experimental uncertainties. Summary and conclusions are given in sect. V.

II. UNITARY CHIRAL THEORY AND THE TWO $\Lambda(1405)$'S

In [5, 6, 7, 8], the unitary formalism with coupled channels using chiral Lagrangians is exposed. The lowest order chiral Lagrangian for the interaction of the pseudoscalar mesons of the SU(3) octet of the pion with the baryons of the proton octet is used. By picking the terms that contribute to the $MB \to MB$ amplitude the La-

*E-mail address: lsgeng@ific.uv.es
†E-mail address: oset@ific.uv.es

grangian is given by [5]:

$$\mathcal{L} = \frac{1}{4f^2}\langle \bar{B} i\gamma^\mu [\Phi\partial_\mu\Phi - \partial_\mu\Phi\Phi, B]\rangle, \quad (1)$$

which, after projected over s-wave, provides tree level transition amplitudes:

$$V_{ij} \;=\; -C_{ij}\frac{1}{4f^2}(k^0 + k'^0), \quad (2)$$

with $k^0(k'^0)$ the energy of the initial(final) meson and C_{ij} are the coefficients tabulated in [5]. These tree level amplitudes are used as kernel of the Bethe-Salpeter equation in coupled channels

$$T = [1 - VG]^{-1}V, \quad (3)$$

where V appears factorized on shell [5, 7] and G is the loop function of a meson and a baryon:

$$\begin{aligned} G &= i\int \frac{d^4q}{(2\pi)^4}\frac{M}{E(\vec{q})}\frac{1}{\sqrt{s} - q^0 - E(\vec{q}) + i\epsilon}\frac{1}{q^2 - m^2 + i\epsilon} \\ &= \int \frac{d^3q}{(2\pi)^3}\frac{1}{2\omega(\vec{q})}\frac{M}{E(\vec{q})}\frac{1}{\sqrt{s} - \omega(\vec{q}) - E(\vec{q}) + i\epsilon}, \end{aligned} \quad (4)$$

which is regularized by a cut off in [5] and in dimensional regularization in [6, 7, 8].

For the particular case of $1/2^-$ states (in MB s-wave interaction) with strangeness $S = -1$ and zero charge one has ten coupled channels: K^-p, $\bar{K}^0n$, $\pi^0\Lambda$, $\pi^0\Sigma^0$, $\eta\Lambda$, $\eta\Sigma^0$, $\pi^+\Sigma^-$, $\pi^-\Sigma^+$, $K^+\Xi^-$, and $K^0\Xi^0$. The explicit solution of the Bethe-Salpeter equation leads to poles in the second Riemann sheet corresponding to resonances. In this sector one finds two poles close to the nominal $\Lambda(1405)$ resonance, and other poles corresponding to the $\Lambda(1670)$- and other Σ- resonances [6, 8].

In Ref. [8], it was shown that the SU(3) decomposition of the $1/2^+$ baryon octet and the pseudoscalar meson octet leads to a singlet and two octets, apart from the 10, $\overline{10}$, and 27 representations. The two octets are degenerate in the limit of exact SU(3) symmetry, but the use of the physical meson and baryon masses breaks explicitly the SU(3) symmetry and thus the degeneracy. As a result, two branches for $I = 0$ and two for $I = 1$ emerge. One of the $I = 0$ branch moves to low energies and comes closer to the singlet at the region of the nominal $\Lambda(1405)$. Reactions occurring in this region, thus, would involve both resonances but only an apparent bump would be seen, giving the impression that there is only one resonance. However, thanks to the very different couplings of the two poles to the $\bar{K}N$ and $\pi\Sigma$ channels, and also since the low-energy pole is broader than the high-energy pole, the shape of the bump seen is likely to change from one reaction to another.

III. THE $pp \to pK^+\Lambda(1405)$ REACTION MECHANISMS

In this section, we investigate the possible $pp \to pK^+\Lambda(1405)$ reaction mechanisms. We concentrate on the final decay state $\pi^0\Sigma^0$ of the $\Lambda(1405)$ in order to compare with the experimental results of [23]. Assuming an s-wave for the final states, which are close to threshold, conservation of spin and parity dictates that the initial proton-proton system, with isospin $I = 1$, has total angular momentum $L = 0$ and total spin $S = 0$; therefore, the pp spin wave function can be written as

$$|pp\rangle = \frac{1}{\sqrt{2}}(|1/2, -1/2\rangle - |-1/2, 1/2\rangle). \quad (5)$$

With incident protons of laboratory momentum 3.65 GeV/c, the $pp \to pK^+\Lambda(1405)$ reaction can occur through kaon, pion, and rho meson exchanges, as shown in Figs. 1, 2, and 3.

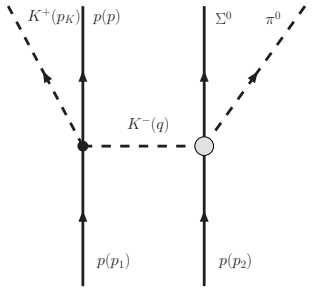

FIG. 1: The kaon exchange mechanism of the $pp \to pK^+\Lambda(1405)$ reaction.

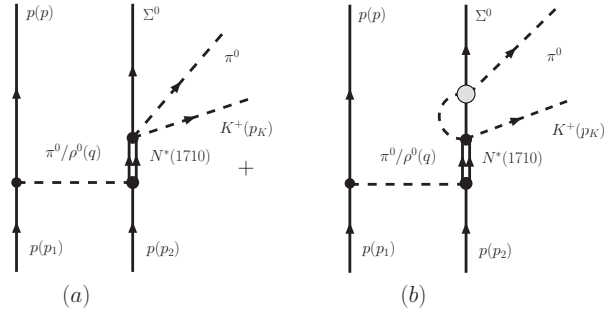

FIG. 2: The pion (rho) exchange mechanism of the $pp \to pK^+\Lambda(1405)$ reaction through N^* excitation.

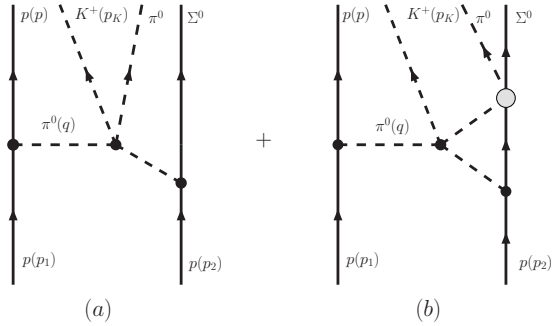

FIG. 3: The pion exchange mechanism of the $pp \to pK^+\Lambda(1405)$ reaction through meson cloud.

TABLE I: The $N^* \to K^+ MB$ couplings with MB one of the ten coupled channels.

MB	K^-p	$\bar{K}^0 n$	$\pi^0\Lambda$	$\pi^0\Sigma^0$	$\eta\Lambda$	$\eta\Sigma^0$	$\pi^+\Sigma^-$	$\pi^-\Sigma^+$	$K^+\Xi^-$	$K^0\Xi^0$
C	2	1	$\frac{\sqrt{3}}{2}$	$\frac{1}{2}$	$\frac{3}{2}$	$\frac{\sqrt{3}}{2}$	0	1	0	0

Kaon exchange at low energies for the reaction proceeds as depicted in Fig. 1, where on one nucleon one has the $K^-p \to K^-p$ amplitude in s-wave, while on the other nucleon one has the $\Lambda(1405)$ production via $K^-p \to \Lambda(1405) \to \pi^0\Sigma^0$. With the strong vertices given in the appendix, the corresponding t matrix element reads:

$$t_K = -\frac{1}{2f_K^2}(q^0 - \omega_{K^+})\frac{1}{q^{02} - \vec{q}^2 - m_K^2} t_{K^-p\to\pi^0\Sigma^0}. \quad (6)$$

For the pion exchange mechanism we would have the Yukawa vertex on one nucleon while the $\pi^0 p \to K^+\Lambda(1405) \to K^+\pi^0\Sigma^0$ reaction on the other nucleon. For this latter amplitude we follow the method of Ref. [18] and we have the mechanisms shown in Figs. 2 and 3, where the pion excites the $N^*(1710)$ resonance, Fig. 2, or interacts with a meson cloud, Fig. 3. In Ref. [18] in this latter case the meson pole amplitude was accompanied with the contact term, and cancellations between the off shell part of the meson pole term and the contact term were pointed out there. Here we make explicit use of this finding and we evaluate only the meson pole term, by taking the meson meson amplitude on shell (i.e., as a function of the meson meson invariant mass and replacing p_i^2 by m_i^2 for the meson legs).

The t matrix element corresponding to pion exchange through N^* excitation (Fig. 2) reads

$$t_\pi = -\frac{g_A}{2f_\pi}\vec{q}^2 \frac{1}{q^{02} - \vec{q}^2 - m_\pi^2} \frac{1}{\sqrt{s'} - M_{N^*} + i\frac{\Gamma}{2}} \frac{AB}{f_\pi^3} \times \left[C_{\pi^0\Sigma^0}(\omega_{\pi^0} - \omega_{K^+}) + \sum_i C_i(\omega_i - \omega_{K^+}) G_i t_{i\to\pi^0\Sigma^0} \right], \quad (7)$$

where s' is the invariant energy squared of the $N^*(1710)$ determined by

$$s' = (p_1 + p_2 - p)^2 = s + M_N^2 - 2\sqrt{s}E(p), \quad (8)$$

G_i are the one-meson one-baryon loop functions of Eq. (4), C_i the coupling constants tabulated in Table I, and i one of the ten coupled channels. A and B are the coupling constants of the $N^*(1710)$ decaying into baryon-meson and baryon-meson-meson as defined in the appendix and in Ref. [18]. Their numerical values are given below. The amplitudes $t_{MB\to MB}$ are the meson-baryon meson-baryon amplitudes described in sec. II. Finally, the t-matrix element corresponding to pion exchange through meson cloud (Fig. 3) reads

$$t_{\rm MP} = \frac{g_A}{2f_\pi}\vec{q}^2 \frac{1}{q^{02} - \vec{q}^2 - m_\pi^2} \left[\mathcal{M}_4 + \sum_i \mathcal{M}_i G_i t_{i\to 4} \right] \quad (9)$$

with the amplitudes $\mathcal{M}_i$ given in the appendix.

The $N^*(1710)$ decay coupling constants A and B appearing in Eq. (7) are fixed by the $N^*(1710)$ partial decay widths into $\pi\pi N$ and πN. Considering the rather large uncertainty of the $N^*(1710)$ total decay width and the corresponding branching ratios [26], we choose two sets of parameters: For parameter set I, we take $M_{N^*} = 1740\,$MeV, $\Gamma = 200\,$MeV, $\Gamma_{\pi\pi N} = 100\,$MeV, $\Gamma_{\pi N} = 40\,$MeV, which yield $A = 0.11$ and $B = 0.84$; for parameter set II, we take $M_{N^*} = 1710\,$MeV, $\Gamma = 100\,$MeV, $\Gamma_{\pi\pi N} = 65\,$MeV, $\Gamma_{\pi N} = 15\,$MeV, which yield $A = 0.07$ and $B = 0.77$. A recent combined analysis [27] of different reactions also require the presence of the $N^*(1710)$ but it has not improved on the present uncertainties of the properties of this resonance. For the energy evolution of the N^* decay width, we have taken into account the effects of the Blatt-Weisskopf penetration factors [28, 29].

The N^* excitation mechanism can also be induced by ω or ρ meson exchange (see Fig. 2). We note that the latest study of [30] shows that the branching ratio of the $N^*(1710)$ decaying into $N\omega$ is only 0.2%, instead of $(13.0 \pm 2.0)\%$, as quoted by the PDG [26], deduced by the same authors as in [30] in an earlier work [31]. Therefore, we will not consider the N^* excitation induced by an ω meson. According to the PDG [26], the branching ratio of the $N^*(1710)$ decaying into $N\rho$ is $5 - 25\%$. With the standard strong vertices as shown in the appendix, the t-matrix element of the ρ induced N^* excitation reads

$$t_\rho = t_\rho^{(1)} + t_\rho^{(2)} \frac{(\sigma^{(1)} \times \vec{q})(\sigma^{(2)} \times \vec{q})}{\vec{q}^2} \quad (10)$$

with

$$t_\rho^{(1)} = -\mathcal{N}^2 \left\{ \left[G^V - \frac{\vec{q}^2}{2M(E+M)} G^T \right] \left(1 - \frac{q^{02}}{m_\rho^2} \right) + \frac{G^V \vec{q}^2}{(E+M)^2} \left(1 + \frac{\vec{q}^2}{m_\rho^2} \right) + \frac{G^T}{2M(E+M)^2} \frac{q^0 \vec{q}^4}{m_\rho^2} \right\} \times \frac{1}{q^{02} - \vec{q}^2 - m_\rho^2} G_{\rho N N^*} \frac{1}{\sqrt{s'} - M_{N^*} + i\frac{\Gamma}{2}} \frac{B}{f_\pi^2} \times \left[C_{\pi^0\Sigma^0}(\omega_{\pi^0} - \omega_{K^+}) + \sum_i C_i(\omega_i - \omega_{K^+}) G_i t_{i\to\pi^0\Sigma^0} \right],$$

$$t_\rho^{(2)} = \mathcal{N}^2 \frac{\vec{q}^2}{E+M} \left(\frac{G^V}{E+M} + \frac{G^T}{2M} \right) \times \frac{1}{q^{02} - \vec{q}^2 - m_\rho^2} G_{\rho N N^*} \frac{1}{\sqrt{s'} - M_{N^*} + i\frac{\Gamma}{2}} \frac{B}{f_\pi^2} \times$$

$$\left[C_{\pi^0\Sigma^0}(\omega_{\pi^0}-\omega_{K^+})+\sum_i C_i(\omega_i-\omega_{K^+})G_i t_{i\to\pi^0\Sigma^0}\right]$$

where $\mathcal{N}=\sqrt{\frac{E+M}{2M}}$; E and M are the energy and mass of the initial protons.

The value of the coupling constant $G_{\rho NN^*}$ in the $G_{\rho NN^*}\gamma^\mu\epsilon_\mu\vec{\tau}\cdot\vec{\rho}$ vertex is determined by reproducing the $N^*(1710)$ decay width into $N\rho$ ($\sim 15\,\mathrm{MeV}$). Its sign, however, cannot be fixed. Therefore, we will present results corresponding to both cases. Taking into account the relatively large widths of the $N^*(1710)$ and the rho, we used the following double convolution to obtain the $N^*(1710)$ decay width into $N\rho$:

$$\begin{aligned}\Gamma_\rho &= \frac{3}{C}\int_{M_{N^*}-2\Gamma}^{M_{N^*}+2\Gamma} d\tilde{M}\int_{m_\rho-2\Gamma_\rho}^{m_\rho+2\Gamma_\rho} d\tilde{m}_\rho \\ &\times\frac{1}{\pi}\mathrm{Im}\frac{1}{\tilde{M}-M_{N^*}+i\Gamma/2}G^2_{\rho NN^*} \\ &\times\frac{1}{\pi}\mathrm{Im}\frac{1}{\tilde{m}_\rho-m_\rho+i\Gamma_\rho/2}\Theta(\tilde{M}-\tilde{m}_\rho-M) \\ &\times\frac{1}{2\pi}\frac{M}{\tilde{M}}q\left(-\frac{3}{2}+\frac{E-q^0}{2M}+\frac{q^0(\tilde{M}^2-M^2)}{2M\tilde{m}_\rho^2}\right),\end{aligned} \tag{11}$$

where Θ is the step function, q is the 3-momentum of $N\rho$ in the rest frame of the $N^*(1710)$, E and M the nucleon energy and mass, the factor 3 accounts for isospin, and C is the normalization constant

$$\begin{aligned}C &= \int_{M_{N^*}-2\Gamma}^{M_{N^*}+2\Gamma} d\tilde{M}\int_{m_\rho-2\Gamma_\rho}^{m_\rho+2\Gamma_\rho} d\tilde{m}_\rho\frac{1}{\pi}\mathrm{Im}\frac{1}{\tilde{M}-M_{N^*}+i\Gamma/2} \\ &\times\frac{1}{\pi}\mathrm{Im}\frac{1}{\tilde{m}_\rho-m_\rho+i\Gamma_\rho/2}\Theta(\tilde{M}-\tilde{m}_\rho-M).\end{aligned} \tag{12}$$

For the mass and width of the $N^*(1710)$ appearing in the above equation, we use the N^* parameter set I.

With incident protons of lab momentum 3.65 GeV/c, the exchanged pion and rho are very much off shell, which must be taken into account in a realistic study. For the pion exchange diagram, we multiply the πNN vertex by the following recoil correction

$$R(q)=1-\frac{q^0}{2M} \tag{13}$$

with q outgoing from the nucleon and the form factor

$$F(q)=\frac{\Lambda_\pi^2-m_\pi^2}{\Lambda_\pi^2-q^2} \tag{14}$$

with $\Lambda_\pi=1.0\,\mathrm{GeV}$. For the πNN^* vertex, we multiply the same form factor but with the recoil correction:

$$R(q)=1+\frac{q^0}{2M}, \tag{15}$$

since q is now incoming. For the ρNN and ρNN^* vertices, following Ref. [32], we multiply a form factor of the dipole form

$$F(q)=\left(\frac{\Lambda_\rho^2-m_\rho^2}{\Lambda_\rho^2-q^2}\right)^2 \tag{16}$$

with $\Lambda_\rho=2\,\mathrm{GeV}$. As for the kaon exchange diagram, taking into account relativistic correction, the $p\to pKK$ vertex becomes

$$-it=i\frac{1}{2f_K^2}(\omega_{K^-}-\omega_{K^+}-E_N+M_N). \tag{17}$$

We also multiply this vertex with a form factor of the form

$$F(q)=\frac{\Lambda_K^2-m_K^2}{\Lambda_K^2-q^2} \tag{18}$$

with $\Lambda_K=1.25$ GeV. A moderate modification of all the cutoff values, Λ_π, Λ_ρ, and Λ_K, will not change our results significantly, as will be shown below.

IV. RESULTS AND DISCUSSION

With all the t-matrix elements provided above, the invariant mass distribution is then calculated by

$$\begin{aligned}\frac{d\sigma}{dM_{\pi^0\Sigma^0}} &= \frac{1}{32\pi^5}\frac{M_N^3M_{\Sigma^0}}{\sqrt{s^2-4sM_N^2}}\int dE\int d\omega\,\Theta(1-\cos^2\theta) \\ &\times\tilde{k}\Big\{[2(t_K+t_\rho^{(1)})]^2+2[2t_\rho^{(2)}]^2 \\ &+[2(t_\pi+t_{\mathrm{MP}})]^2\Big\},\end{aligned} \tag{19}$$

with $\tilde{k}$ the π^0 (Σ^0) 3-momentum in the center-of-mass frame of $\pi^0\Sigma^0$ and θ the angle between $\vec{p}$ and $\vec{p}_K$ given by

$$\tilde{k}=\frac{\lambda^{1/2}(M^2_{\pi^0\Sigma^0},m^2_{\pi^0},M^2_{\Sigma^0})}{2M_{\pi^0\Sigma^0}}, \tag{20}$$

$$\cos\theta=\frac{(\sqrt{s}-E-\omega)^2-\vec{p}^{\,2}-\vec{p}_K^{\,2}-M^2_{\pi^0\Sigma^0}}{2|\vec{p}||\vec{p}_K|}, \tag{21}$$

where E and ω are the energies of the final proton and K^+. The factors 2 in Eq. (19) accounts for the possibility of having the $\Lambda(1405)$ production from either of the two protons.

It is to be noted that although Ref. [23] only measured the $\pi^0\Sigma^0$ final state, the total cross section given in Ref. [23] is for $\Lambda(1405)\to\pi\Sigma$, which implies that a factor of 3 has been multiplied to account for the isospin. To compare with the data, we have multiplied our invariant mass distribution , Eq. (19), with the same factor to obtain the distribution of the $\pi\Sigma$.

In Fig. 4, the calculated invariant mass distribution of the $\Lambda(1405)$ with N^* parameter sets I and II are compared with the new data of Ref. [23]. The shaded area indicates the uncertainties of our calculation related to the determination of the N^* coupling constants A and B. For demonstration purposes, we did not include the ρ exchange contribution. It is seen that within the experimental uncertainties, our calculations reproduce the data rather well, particularly the fast drop at the $\bar{K}N$ threshold. Although both parameter sets reproduce the data very well, in particular taking into account the large experimental uncertainties, we would say that parameter set I is preferred, which is in agreement with the finding of Ref. [18]. In the following, we would use parameter set I as our default choice.

Now we would like to study the contribution of the ρ exchange. The coupling constant $G_{\rho NN^*}$ is fixed to reproduce the estimated $N^*(1710)$ decay width into $N\rho$, $\sim 15\,\mathrm{MeV}$, which yields $|G_{\rho NN^*}| = 0.62$. Its sign, however, cannot be fixed. In Fig. 5, we present the calculated invariant mass distribution corresponding to both cases, i.e. $G_{\rho NN^*} = -0.62$ and $G_{\rho NN^*} = 0.62$. It is seen that both reproduce the data rather well, in other words, the quality of the present data cannot discriminate the sign of $G_{\rho NN^*}$. We further notice that our calculated total cross section $\sim 5\ \mu b$ is also in good agreement with the data $4.5 \pm 0.9 \pm 1.8\ \mu b$.

In Fig. 6, the contribution of the kaon exchange mechanism and those of the pion and rho exchanges are compared. It can be clearly seen that the kaon exchange mechanism leads to an asymmetric peak at $\sim 1410\,\mathrm{MeV}$, while the pion exchange mechanism broadens the shape and leads to a better agreement with the data. We would like to stress that the ρ exchange contribution by itself is very small, only through the interference with the kaon contribution its effect becomes relevant.

The broad shape of the pion exchange mechanism is actually made by the collaboration of three very different contributions as can be seen in Fig. 7. One comes from the tree level diagram (diagram (a) of Fig. 2), which peaks at low invariant masses. Another one is from the mechanism with re-scattering (diagram (b) of Fig. 2), which is dominated by the broad $\Lambda(1405)$ pole of low energy. Finally the mechanism of the meson pole, Fig. 3, is dominated by the narrow high energy pole of the $\Lambda(1405)$. The coherent sum of all these mechanisms produces the broad shape shown in Fig. 6. One can see in this figure that the pion exchange term provides strength for the $pp \to K^+\pi^0\Sigma^0$ reaction in the low energy side of the invariant mass, leading to an apparent broader width of the $\Lambda(1405)$ compared with the one we would obtain from the K exchange mechanism alone, which is mostly dominated by the high energy $\Lambda(1405)$ pole.

It is interesting to note that the strong amplitudes $t_{MB\to MB}$ are determined by the very precise $\bar{K}N$ branching ratios r, R_c, and R_n [5]; therefore, most uncertainties in our model come from the $N^*(1710)$ coupling constants A, B, and $G_{\rho NN^*}$, which are partly shown in Figs. 4 and

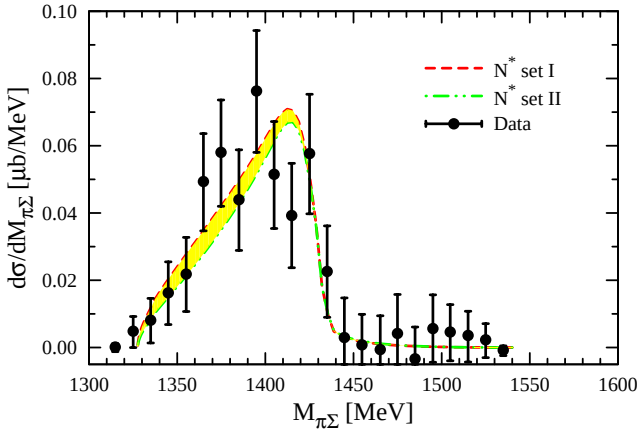

FIG. 4: The invariant mass distribution of the $\pi\Sigma$ in comparison with the data [23]. The ρ exchange contribution is not included.

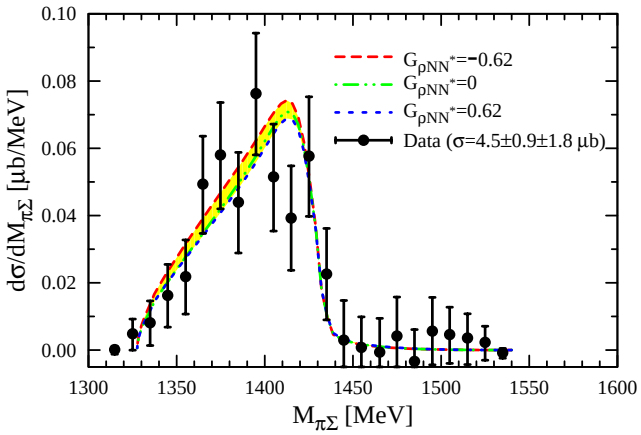

FIG. 5: The invariant mass distribution of the $\pi\Sigma$ in comparison with the data [23].

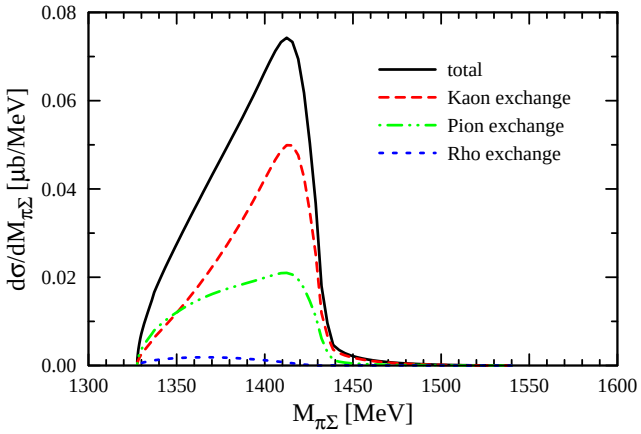

FIG. 6: The contribution of the three different mechanisms with $G_{\rho NN^*} = -0.62$.

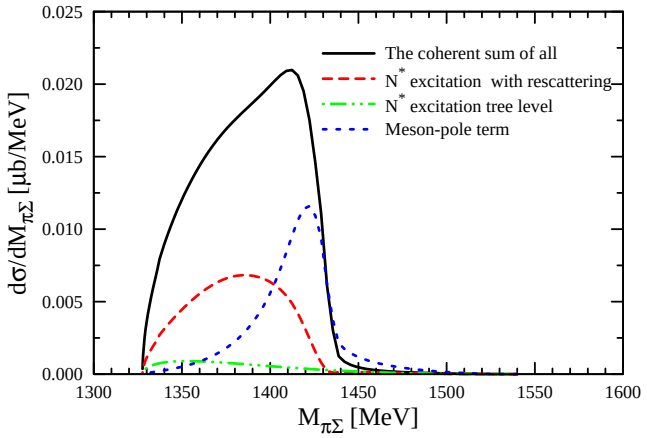

FIG. 7: The components of the π exchange contribution. See text for details.

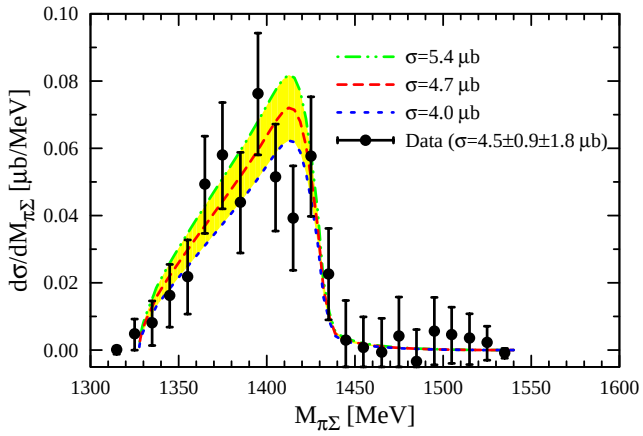

FIG. 8: The invariant mass distribution of the $\pi\Sigma$ with theoretical uncertainties estimated using Monte-Carlo sampling method (see text for details), in comparison with the data [23].

5, and the form factors which take into account the off-shellness of the exchanged particles.

To estimate the theoretical uncertainties related to the $N^*(1710)$ decay widths and the cutoff values, we perform a Monte-Carlo sampling of the parameter values within their uncertainties, more specifically, we allow the $N^*(1710)$ total width to vary in the range of 200 ± 30 MeV, $\Gamma_{\pi\pi N}$ in the range of 100 ± 15 MeV, $\Gamma_{\pi N}$ in the range of 40 ± 6 MeV, $\Gamma_{\rho N}$ in the range of 5-25 MeV, Λ_π within 1.0 ± 0.1 GeV, Λ_ρ within 2.0 ± 0.2 GeV, while Λ_K within 1.25 ± 0.125 GeV. Since $G_{\rho N N^*}$ can have either negative or positive sign, we assign half of the Monte-Carlo generated values positive sign and half of them negative sign. The so-obtained averaged invariant mass distribution and the band corresponding to $\bar{y} \pm \sigma$ with $\bar{y} = \frac{1}{N}\sum y_i$ and $\sigma^2 = \frac{1}{N-1}\sum (y_i - \bar{y})^2$ are displayed in Fig. 8. The total cross section is estimated to be $4.7 \pm 0.7\,\mu$b, which should be compared with the data: $4.5 \pm 0.9 \pm 1.8\ \mu b$ [23].

The strength of the present reaction has brought a new information concerning the kaon exchange diagram in Fig. 1, where we implemented a form factor in the $pK\bar{K}$ vertex. Should we have not taken this form factor into account, the contribution of the kaon exchange, which is the dominant mechanism, would have been larger and the cross section would have been about a factor of three times bigger than what we have evaluated. We can state this, but cannot be more conclusive with respect to the shape of the form factor, Eq. (18), because the present experiment selects only one value of q^2 approximately, $q^2 \approx -|\vec{p}_1|^2 \approx -(1150\,\text{MeV})^2$. Similarly, we cannot induce whether a form factor should be implemented in only one or both vertices of the kaon exchange. All that the experiment is telling us is that for the off-shellness of this process, with $q^2 \approx -(1150\,\text{MeV})^2$, the kaon exchange amplitude is reduced by about a factor of two with respect to the ordinary kaon exchange with no form factors.

V. SUMMARY AND CONCLUSIONS

We have performed a theoretical study of the $pp \to pK^+\Lambda(1405)$ reaction recently investigated at COSY-Jülich. Based on unitary chiral theory, we constructed a model including three different mechanisms: single-kaon exchange, single-pion exchange, and single-rho exchange. We showed that the kaon exchange mechanism was mostly sensitive to the high energy pole of the $\Lambda(1405)$ and produced by itself a relatively narrow structure. Yet, the mechanism of pion exchange, itself a combination of various terms, provided a different shape for the $\pi^0\Sigma^0$ invariant mass, that added to the one of kaon exchange had the effect of producing strength in the low invariant mass part, resulting in a broadening of the invariant mass distribution and a better agreement with experiment. The rho exchange contribution has a similar (but smaller) effect as the pion exchange if the sign of $G_{\rho N N^*}$ is negative.

The total strength of the cross section demanded a reduction of the dominant kaon exchange mechanism, where the kaon appears largely off shell. The reduction is of the order of a factor of two in the amplitude for $q^2 \approx -(1150\,\text{MeV})^2$. Thus we introduced a monopole form factor with $\Lambda_K \approx 1.25$ GeV, which is of natural size. With this value chosen, an error analysis was performed by changing input parameters within experimental boundaries, or changing the cutoff parameters of the form factors by about 10% of their central values. The result is a band of cross sections with a certain dispersion at low invariant masses, compatible with experiment, and a fast fall down around 1430 MeV, rather independent of the input, which is also clearly seen in the data.

Once more we show in this paper that the association of a shape of the $\pi^0\Sigma^0$ distribution to a universal $\Lambda(1405)$ resonance is a delicate subject and that one should rather make a thorough study of the different reaction mecha-

nisms entering the process, since the observed final shape is a subtle combination of contributions from background and the two $\Lambda(1405)$ poles which are weighted differently in the various mechanisms.

VI. ACKNOWLEDGMENTS

We would like to acknowledge useful discussions with I. Zychor, H. Ströher, and particularly the lengthy and instructive discussions with C. Wilkin. L. S. Geng acknowledges financial support from the Ministerio de Educacion y Ciencia in the Program of estancias de doctores y tecnologos extranjeros. This work is partly supported by DGICYT contract number FIS2006-03438 and the Generalitat Valenciana. This research is part of the EU Integrated Infrastructure Initiative Hadron Physics Project under contract number RII3-CT-2004-506078.

Appendix

For the strong vertices, we have used the following Feynman rules:

1. $p \to p\pi^0$:

$$-it = -\frac{g_A}{2f_\pi}\vec{\sigma}\cdot\vec{q}. \tag{22}$$

2. $p\pi^0 \to N^*$:

$$-it = \frac{A}{f_\pi}\vec{\sigma}\cdot\vec{q}. \tag{23}$$

3. $p\rho \to N^*$:

$$-it = iG_{\rho NN^*}\bar{\psi}\gamma^\mu\vec{\tau}\cdot\vec{\epsilon}_\mu\psi. \tag{24}$$

4. $p \to p\rho$:

$$-it = -i\bar{\psi}\left\{G^V\gamma^\mu + G^T\frac{1}{2im_p}\sigma^{\mu\nu}q_\nu\right\}\vec{\tau}\cdot\vec{\epsilon}_\mu\psi, \tag{25}$$

with $G^V = 2.9 \pm 0.3$ and $G^T/(2m_p) = 1.35 \pm 0.12\, m_\pi^{-1}$, which provide $G^T/G^V = 6.27$ [33].

5. $N^* \to K^+MB$:

$$-it = i\frac{B}{f_\pi^2}C_{MB}(\omega_M - \omega_{K^+}), \tag{26}$$

with the C_{MB} couplings tabulated in Table I.

6. $p \to pK^+K^-$:

$$-it = i\frac{1}{2f_K^2}(\omega_{K^-} - \omega_{K^+}). \tag{27}$$

7. $MM \to MM$

$$-it = i\frac{1}{12f_\pi^2}\langle(\partial\Phi\Phi - \Phi\partial\Phi)^2 + M\Phi^4\rangle, \tag{28}$$

with Φ the meson octet and M the quark mass matrix.

8. $MB \to B$

$$-it = i\left[\frac{D+F}{2}\langle\bar{B}\gamma^\mu\gamma_5 u_\mu B\rangle + \frac{D-F}{2}\langle\bar{B}\gamma^\mu\gamma_5 B u_\mu\rangle\right], \tag{29}$$

with B the baryon octet of the proton. In the present work, the following parameter values have been used: $f_\pi = 93$ MeV, $f_K = 1.22 f_\pi$, $g_A = 1.26$, $D = 0.795$, and $F = 0.465$.

When calculating the meson-pole diagram, as explained in detail in Ref. [18], one can put the $MMMM$ vertex on shell, the off shell part after canceling a meson-propagator, will be canceled by the $MMBBB$ contact term [18]. Furthermore, with the present experimental setup, one can assume that the outgoing mesons and baryons are almost at rest, which we take for the evaluation of matrix elements. Below, we give the meson-pole amplitudes appearing in Eq. (9) in the order of K^-p, $\bar{K}^0n$, $\pi^0\Lambda$, $\pi^0\Sigma^0$, $\eta\Lambda$, $\eta\Sigma^0$, $\pi^+\Sigma^-$, $\pi^-\Sigma^+$, $K^+\Xi^-$, and $K^0\Xi^0$:

$$\mathcal{M}_1 = \mathcal{M}_1^\pi + \mathcal{M}_1^\eta, \tag{30}$$

$$\mathcal{M}_1^\pi = -\frac{D+F}{6f_\pi^3}\frac{s_1}{D_1(m_\pi)}, \tag{31}$$

$$\mathcal{M}_1^\eta = \frac{D-3F}{24f_\pi^3}\frac{1}{D_1(m_\eta)} \times\left[3s_1 - \frac{1}{3}m_\pi^2 - m_\eta^2 - \frac{8}{3}m_K^2\right], \tag{32}$$

$$\mathcal{M}_3 = \frac{3F+D}{12\sqrt{3}f_\pi^3}\frac{1}{D_3(m_K)} \times\left[-s_3 + 2(m_\pi^2 + m_K^2) - \frac{(m_K^2 - m_\pi^2)^2}{s_3}\right], \tag{33}$$

$$\mathcal{M}_4 = \frac{F-D}{12f_\pi^3}\frac{1}{D_4(m_K)} \times\left[-s_4 + 2(m_\pi^2 + m_K^2) - \frac{(m_K^2 - m_\pi^2)^2}{s_4}\right], \tag{34}$$

$$\mathcal{M}_5 = \frac{3F+D}{24f_\pi^3}\frac{1}{D_5(m_K)} \times\left[-\frac{3}{2}s_5 - \frac{(m_\pi^2 - m_K^2)(m_\eta^2 - m_K^2)}{2s_5} + \frac{7}{6}m_\pi^2 + \frac{m_\eta^2}{2} + \frac{1}{3}m_K^2\right], \tag{35}$$

$$\mathcal{M}_6 = \frac{\sqrt{3}(F-D)}{24f^3}\frac{1}{D_6(m_K)} \times\left[-\frac{3}{2}s_6-\frac{(m_\pi^2-m_K^2)(m_\eta^2-m_K^2)}{2s_6} +\frac{7}{6}m_\pi^2+\frac{m_\eta^2}{2}+\frac{1}{3}m_K^2\right], \quad (36)$$

$$\mathcal{M}_8 = \frac{D-F}{4f_\pi^3}\frac{1}{D_8(m_K)} \times\left[s_8-m_\pi^2-m_K^2+\frac{s_8^2-(m_K^2-m_\pi^2)^2}{2s_8}\right], \quad (37)$$

$$\mathcal{M}_2=\mathcal{M}_7=\mathcal{M}_9=\mathcal{M}_{10}=0. \quad (38)$$

The meson propagator is given by

$$\frac{1}{D_i(m)}=\frac{1}{(q^0-\omega_i-m_K)^2-\vec{q}^2-m^2}, \quad (39)$$

with the energy of the meson ω_i and the invariant mass squared of the meson-pair s_i given by

$$\omega_i=\frac{M_I^2+m_i^2-M_i^2}{2M_I}, \quad (40)$$

$$s_i=(m_K+M_I-M_i)^2, \quad (41)$$

where M_I is the invariant mass of the $\Lambda(1405)$ and m_i (M_i) the meson (baryon) mass of channel i. The last equation, Eq. (41), is obtained assuming final particles with small momentum, in line with the comments made above, and is sufficiently good for our purpose.

[1] N. Isgur and G. Karl, Phys. Rev. **D18**, 4187 (1978).
[2] R. H. Dalitz and S. F. Tuan, Phys. Rev. Lett. **2**, 425 (1959).
[3] R. H. Dalitz and S. F. Tuan, Annals Phys. **10**, 307 (1960).
[4] N. Kaiser, T. Waas, and W. Weise, Nucl. Phys. **A612**, 297 (1997).
[5] E. Oset and A. Ramos, Nucl. Phys. **A635**, 99 (1998).
[6] E. Oset, A. Ramos, and C. Bennhold, Phys. Lett. **B527**, 99 (2002).
[7] J. A. Oller and U. G. Meissner, Phys. Lett. **B500**, 263 (2001).
[8] D. Jido, J. A. Oller, E. Oset, A. Ramos, and U. G. Meissner, Nucl. Phys. **A725**, 181 (2003).
[9] C. Garcia-Recio, J. Nieves, E. Ruiz Arriola, and M. J. Vicente Vacas, Phys. Rev. **D67**, 076009 (2003).
[10] C. Garcia-Recio, M. F. M. Lutz, and J. Nieves, Phys. Lett. **B582**, 49 (2004).
[11] T. Hyodo, S. I. Nam, D. Jido, and A. Hosaka, Phys. Rev. **C68**, 018201 (2003).
[12] B. Borasoy, R. Nissler, and W. Weise, Eur. Phys. J. **A25**, 79 (2005).
[13] J. A. Oller, J. Prades, and M. Verbeni, Phys. Rev. Lett. **95**, 172502 (2005).
[14] J. A. Oller, Eur. Phys. J. **A28**, 63 (2006).
[15] B. Borasoy, U. G. Meissner, and R. Nissler, Phys. Rev. **C74**, 055201 (2006).
[16] J. C. Nacher, E. Oset, H. Toki, and A. Ramos, Phys. Lett. **B455**, 55 (1999).
[17] J. C. Nacher, E. Oset, H. Toki, and A. Ramos, Phys. Lett. **B461**, 299 (1999).
[18] T. Hyodo, A. Hosaka, E. Oset, A. Ramos, and M. J. Vicente Vacas, Phys. Rev. **C68**, 065203 (2003).
[19] L. S. Geng, E. Oset, and M. Doring, Eur. Phys. J. **A32**, 201 (2007).
[20] J. K. Ahn (LEPS), Nucl. Phys. **A721**, 715 (2003).
[21] S. Prakhov et al. (Crystall Ball), Phys. Rev. **C70**, 034605 (2004).
[22] V. K. Magas, E. Oset, and A. Ramos, Phys. Rev. Lett. **95**, 052301 (2005).
[23] I. Zychor et al. (2007), arXiv:0705.1039 [nucl-ex], Phys. Lett. B (in print).
[24] D. W. Thomas, A. Engler, H. E. Fisk, and R. W. Kraemer, Nucl. Phys. **B56**, 15 (1973).
[25] R. J. Hemingway, Nucl. Phys. **B253**, 742 (1985).
[26] W. M. Yao et al. (Particle Data Group), J. Phys. **G33**, 1 (2006).
[27] A. V. Sarantsev et al., Phys. Lett. **B659**, 94 (2008).
[28] D. M. Manley, R. A. Arndt, Y. Goradia, and V. L. Teplitz, Phys. Rev. **D30**, 904 (1984).
[29] D. M. Manley and E. M. Saleski, Phys. Rev. **D45**, 4002 (1992).
[30] P. Muehlich, V. Shklyar, S. Leupold, U. Mosel, and M. Post, Nucl. Phys. **A780**, 187 (2006).
[31] G. Penner and U. Mosel, Phys. Rev. **C66**, 055211 (2002).
[32] R. Machleidt, K. Holinde, and C. Elster, Phys. Rept. **149**, 1 (1987).
[33] E. Oset and M. J. Vicente-Vacas, Nucl. Phys. **A446**, 584 (1985).